Indian Journal of Geo Marine Sciences
Vol. 48 (02), February 2019, pp. 193-204

Environmental pollution and pattern formation of Harsin–Sahneh ophiolitic complex (NE Kermanshah—west of Iran)

Ali Moradpour[1]*, Reza Zarei Sahamieh[2], Ahmad Ahmadi Khalaji[2], & Ramin Sarikhani[2]

[1] Soil Conservation and Watershed Management Research Department, Kermanshah Agricultural and Natural Resources Research and Education Center, AREEO, Kermanshah, Iran

[2]Department of Geology, Faculty of Sciences, Lorestan University, Khoramabad, Iran

*[E-mail: alimoradpour9@gmail.com]

Received: 25 January 2016; revised 28 November 2016

To determine and estimate the environmental impact of certain elements- 10 soil samples from various areas in these massifs have been investigated. The obtained results show that most of heavy and major elements were exceeding the permissible levels in soil samples in the study area. On the subject of soil quality, concentrations of elements Cr, Mn, Fe, Ca, Mg, Ca, Ni, and Zn are above permissible levels. Comparing the concentrations of elements with results of grain size analysis illustrates that the concentrations of Cr, Ni, Fe, Mg, and Co are positively correlated with sand fraction and the concentrations of Al, P, Mn, and Pb are directly proportional with clay fraction in soil samples. Petrographic evidence indicates that this ophiolitic sequence consists of both mantle and crustal suites. In this complex, generally lithologies include harzburgitic and lherzolitic peridotites, isotropic and mylonitic gabbros, dyke complex, basaltic pillow lavas, and small out crop of plagiogranite. The mineral chemistry of Harsin mafic rocks is island arc setting for this part of complex and geochemistry of mafic and ultramafic rocks of Sahneh region displaying P-type mid-ocean ridge basalt (MORB) nature.

[Keywords: Environmental impact, Heavy elements, Tethyan ophiolites, Arc magmatism, P-type MORB, Zagro]

Introduction

Generally three major tectonic elements, Zagros fold-thrust belt, the Sanandaj–Sirjan Zone, and the Urumieh–Dokhtar magmatic arc in western and southwestern parts of Iran, are recognized as being related to the subduction of Southern Neo-Tethyan oceanic crust and the collision of the Arabian plate with the central Iran micro plate. The Urumieh–Dokhtar Magmatic Arc (UDMA) consists of intrusive and extrusive rocks of Eocene–Quaternary age that forms a zone 50 km wide and up to 4 km thick; as a matter of fact, the magmatism of the UDMA occurred chiefly during the Eocene but, after a quiescent period, resumed from Upper Miocene to Plio-Quaternary[1].

The subduction inception of the different parts of Southern Neo-Tethyan oceanic crust beneath the SSZ dates back to the Late Triassic to Late Cretaceous [2, 3].

Heavy and trace metal contamination of soils is one of the important concerns in environmental issues. Natural weathering processes in soils, alike to the formation of secondary minerals or organic degradation/mineralization, have a profound effect on the mobility and bioavailability of trace metals[4]. Ultramafic parent materials (e.g., serpentinite) are associated with high levels of toxic trace elements, particularly nickel, chromium, cobalt, zinc, mercury, and lead. Such regions are therefore generally not suitable for agriculture[5,6]. Soils developed over serpentine showed the highest metal concentrations[7]. The serpentine soils are more enriched in Mg and Fe due to weathering of some specific minerals existing in such geologic environments (e.g., forsterite, fayalite, and serpentines). It has been proved that high concentrations of some elements such as Cr and Ni are due to presence of ultramafic rocks, development of soils over them and also leachate, and loss of mobile elements from soil profiles.

Present study focuses on the environmental impacts, petrology and geochemistry of the Harsin–Sahneh ophiolite as one important key element of the Peri-Arabic ophiolite system between Oman and Turkey. Also ophiolites, in an advanced state of alteration, are one of the most important sources of toxic minerals and elements that may introduce toxic materials into the ecosystem. Environmental studies of soil in the study area show a high degree of metal pollution due to presence of ultramafic rocks.

Materials and Methods

The southern Iranian ophiolites that located along the Main Zagros Thrust Zone recorded the geodynamic evolution of southern Neo-Tethys oceanic branch between the Arabian shield (Gondwana) and the Sanandaj–Sirjan continental block of Iran. Harsin–Sahneh ophiolites with 34º 00´ N to 34º 30´ N and 47º 10´ E to 47º 50´ E coordinates are located along the Main Zagros Thrust (between the Zagros belt and the SSZ; Fig. 1b). This region consists of several elongate elements from the Tethyan domain. These elements are as follows:

The deformed radiolaritic Nappe: Its original substratum is interpreted as a continental rim basin[8,9] with a stratigraphic thickness of about 500m and lying on the top of the Campanian Gurpi formation and the Maastrichtian Amiran flysch[8]. In some regions, radiolarite thrust sheets were emplaced diachronously onto the Arabian platform in Santonian to Maastrichtian times. In the radiolaritic Nappe, proposed by Gharib [10], the oldest age, Liassic, is for the radiolarite exposed along a composite section located in the Gamasiab valley (SW Harsin).

Harsin–Sahneh ophiolites: consists of both mantle and crustal suites, include peridotite (harzburgite and lherzolite), serpentinited peridotite, gabbro (isotropic and mylonitic gabbros), dyke complex, and basaltic pillow lavas; dyke and pillow lava complexes are limited to Tamark and Gashor areas (between Harsin and Nurabad; Fig.1a).The Kermanshah ophiolite was first considered to be a mid-ocean ridge remnant analogous to those of Oman and Neyriz[11]. Delaloye and Desmons[12] suggested the age of the diorites as 86.3 ± 7.8 Ma (i.e., Campanian), while Whitechurch et al.,[13] estimated it as 58 ± 9 Ma. These diorites cut the volcanic rocks and flyshic sediment (located along the Gamasiab River).

Field evidence indicates that peridotites and intrusive ultramafic and gabbroic rocks mainly crop out between Harsin and Sahneh, along the Gamasiab River.They characterized Harsin–Sahneh domain as a mélange with ophiolitic fragments. No sedimentary cover stratigraphically overlying the various ophiolitic rocks is observed in the Kermanshah area. Although some radiolarite layers are interbedded between the pillow basalts of the Gashor unit and around Harsin, the limestones directly overlying serpentinites were dated as Upper Triassic, while the limestones resting on radiolarites overlying the same serpentinites were dated as Malm. The serpentinised peridotites are considered to be mantle material exhumed during the Early Mesozoic break-up of the Neo-Tethyan Ocean[14].

The Bisotoun Unit: consists of 1500 to 3000m shallow water carbonates that are from Late Triassic to Early Late Cretaceous (Cenomanian). Based on stratigraphic evidence Bisotoun Unit principally crops out into two high massifs, namely Kuh-e Bisotoun and Kuh-e Shirez in the north of Kermanshah and Harsin, respectively (Fig. 1c). In Kuh-e Bisotoun, the oldest cropping strata are made up of late Triassic limestone. In Kuh-e Shirez the cherts deposited are on the serpentinites which their topsides are the same as Bisotun Limestone units[9].

Bisotoun Unit is folded and locally thrusted, Based on geodynamic reconstruction models of the area[26], Bisotoun platform developed over a paleo-high continental crust. This platform separated from the Arabian plate by a continental rim basin, namely Harsin Sub-Oceanic basin, hosting the Kermanshah radiolaritic trough.

To evaluate the degree of contamination of soils in relation to trace and heavy elements, 10 soil samples were collected from cultivated and non–cultivated

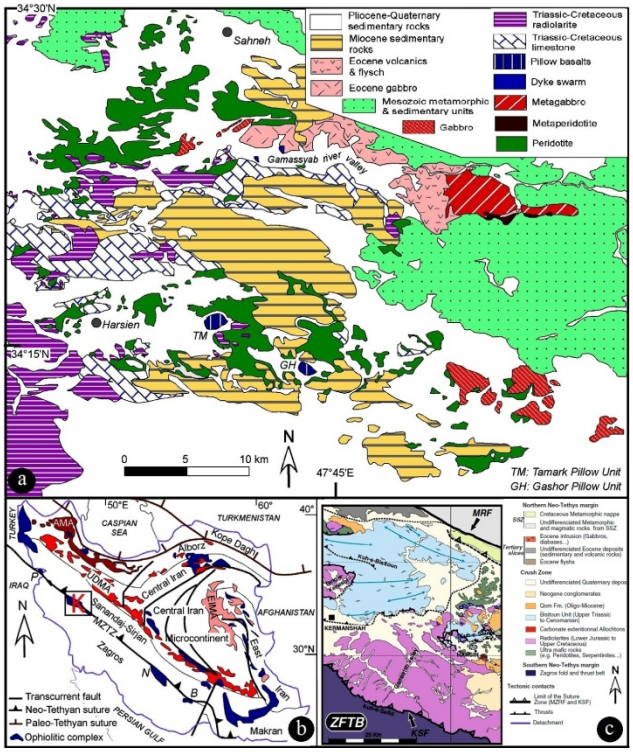

Fig. 1 — A Geological map of the Harsin–Sahneh ophiolite complex (modified after Saccani et al.,[15]) and sampling points. b Structural sketch map of Iran and position of Harsin–Sahneh (K) ophiolite complex (modified after Allahyari et al.,[16]). c Geological map showing the position of Bisotoun unit crops out Kuh-e Bisotoun and Kuh-e Shirez after Wrobel-Daveau et al.,[14]).

sites of the Harsin–Sahneh region. Representative soil samples were collected from a maximum depth of approximately 20 cm .The bulk samples were dried in 60 °C and then were sieved through a <2-mm stainless steel mesh. After dividing the samples to a favorite weight (250 g), milling process was done to reach the particles to the 200 mesh. Heavy metals Cr, Mn, Fe, Al, Ca, P, Mg Co, Ni, Pb, and Zn were analyzed using inductively coupled plasma (ICP) atomic emission spectroscopy and ICP mass spectroscopy. Table 1 shows the analyzed concentration of elements in sampling points. The grain size distribution of soils was determined using a hydrometer method.

The major and trace element composition of gabbroic rock was determined by electron probe micro-analysis (EPMA) using a Cameca SX100 instrument in the Iran Mineral Processing Research Center (IMPRC). Analytical error for major and trace element are 1 and 5% respectively. Analyses average results of 65 points of olivine, plagioclase, and pyroxene are reported in Tables 6.

Whole-rock major and trace element analyses were determined by SGS laboratory (Canada) with ICP-MS and ICP-AES methods. Representative analyses are reported in Table 7.

Also whole-rock major and some trace element analyses for 20 samples (ultramafic and mafic) were obtained by X-ray fluorescence (XRF), using an ARL Advant-XP automated X-ray spectrometer.

In this method, 4 g fraction of each sample was then mixed with 4 mg of lithium tetraborate in a vitreous graphite crucible. Volatile contents were determined as loss on ignition at 1000 °C. Representative analyses are reported in Table 8.

The lowest lithological unit begins with mantle pridotites. Pridotites occurred between Harsin–Sahneh regions. Dunites are not volumetrically most abundant rock in the ultramafic sequence. They generally have a cumulate texture and main grains consist of olivine (more than 90%), enstatite (2–3%), diopside, and diopsidic augite (1–2%) and opaque minerals include Fe-oxide and chromian spinel (less than 2%). The peridotite samples are mainly harzburgite with cumulate texture,composed of olivine (60–70%), orthopyroxene (30–40%), clinopyroxene, and Cr-spinel (1–2%). The presence of kink bands in olivine, orthopyroxene, and clinopyroxene (Fig. 2a) coarse grains is indicative of high temperature plastic mantle deformation [17].

Lherzolites show a porphyry texture. Both pyroxenes show exsolution lamellae along cleavage (Fig. 2b) and kink banding. Cr-spinel crystals in peridotite samples are sub-anhedral (Fig. 2c). In some areas, the peridotite samples have been pervasively altered (serpentinized) to a mixture of lizardite, chrysotile, and brucite; the extensive alteration of peridotite has led to the development of mesh texture (Fig. 2d). In some samples, orthopyroxene (enstatite) is forming asymmetrical kinking and double-hinge disharmonic micro-folds (Fig. 2e).

The gabbro sequences chiefly crop out between Siah chogha valley and Garoos valley. The coarse-grained gabbros show ad-to mesocumulate texture with large crystals of plagioclase (50–60%) clinopyroxene (20–30%) and olivine (10–20%) (Fig. 2f). Mylonitic gabbros are generally coarse grained with mylonitic texture (occurred between Shoveh valley and Garoos valley).

These gabbros occasionally and locally affected by alteration; the secondary minerals are mainly actinolite, tremolite, and epidote. In some samples, scarce clinopyroxene relics are locally preserved, while in other samples porphyroblasts are composed of plagioclase, clinopyroxene, and locally olivine (Fig. 2g). The sampled gabbros are variable in texture; in other words, crystal size ranges from fine grained to coarse grained in these rocks.

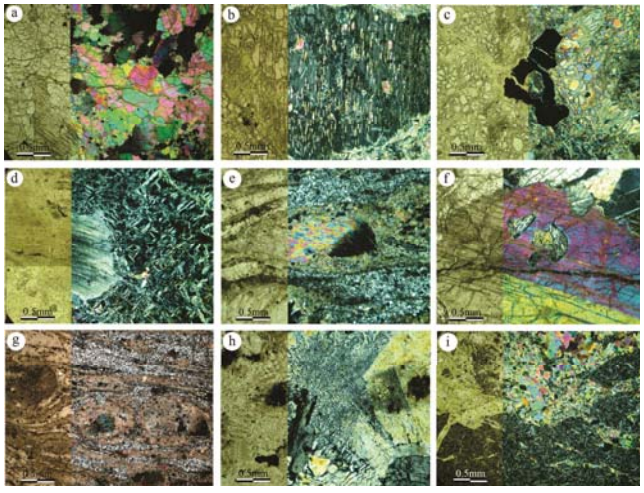

Fig. 2 — Thin section photomicrographs in crossed polarized light and plain polarised light. a. Harzburgite with kink-band in olivine. b. Lamellar exsolution of clinopyroxene in orthopyroxene. c. Chromian spinel crystals in peridotite samples. d. Serpentinized olivine with seive texture in harzburgite. e. Asymmetrical micro-folds and double hinge in orthopyroxene. f. gabbros with pegmatitic texture. g. Clinopyroxene crystals in fine-grained matrix of plagioclase in mylonitic gabbro samples. h. Intergrowths of K-feldspars and quartz, indicating eutectic crystallization at low temperature. i. Aphanitic texture in dyke samples and presence of secondary minerals due to alteration.

The plagiogranite sequence is observable between Sar-Asiaban valley and Darakeh valley. The absence of wide-contact metamorphism around the plagiogranite sequence confirms the low-temperature cooling of the granite magma. Besides, in these samples, there is a graphic texture with intergrowths of K-feldspar + quartz, showing that the plagiogranite sequences are crystallized at low temperatures close to the quartz + K-feldspar eutectic point (Fig. 2h).

The dykes occur between Harsin and Sahneh, crosscutting harzburgites and gabbros. No true sheeted dyke complex exists in the Harsin–Sahneh ophiolites. The texture of the dykes is fine grained and intersertal; the mineral assemblage (e.g., epidote, albite, zeolite, or calcite) depends on the degree of hydrothermal alteration. Pillow basalts display aphyric, fine-grained intergranular and/or sub-ophitic textures. Like dyke samples, the development of the typical mineral assemblage indicate the low degree of hydrothermal alteration conditions (Fig. 2i).

Results

Table 1 illustrates the analyzed concentration of elements in 10 soil sample. The relationships of the studied elements with each other and also soil particle fractions were determined by calculating the correlation coefficients of element pairs and clay, silt, and sand fractions (Table 2). Nonzero correlation coefficient with accompanying $p \leq 0.05$ is considered statistically significant at the 95% confidence limit.

The presence of outliers in the dataset was determined using the Tukey [18] box plot method. It can be seen from Table 2 that elements Co, Ni, and Mg considering the main elements of ultramafic

Table 1 — Concentration of metals (milligrams per kilogram) and grain distribution (percent) of soil samples

sample	Cr	Mn	Fe	Al	Ca	P	Mg	Co	Ni	Pb	Zn	Sand%	Silt%	Clay%
S1	844	821	48900	19200	24500	136	197000	85.7	1470	5.3	64.3	75.8	16.6	7.6
S2	435	1100	50500	70900	46200	868	67100	35.6	346	12.5	93.8	63.4	11.6	25
S3	1080	827	45100	41200	54600	195	135000	53	845	7.9	72.6	74	14	12
S4	717	806	42700	34100	69700	159	136000	60.2	919	8.3	72.1	68	12	20
S5	2600	947	59900	40000	53600	268	122000	53.9	751	6.8	96.2	76.6	12.4	11
S6	1200	882	47200	37800	49000	397	159000	60.2	1010	7.2	72.3	77	13	10
S7	819	969	52900	53000	60500	826	95700	42.3	550	11.1	111	78	1	21
S8	663	997	43400	39100	34200	431	142000	59.1	895	6.9	65.5	56.8	9	34.2
S9	690	739	41100	29900	40100	130	172000	77	1240	6.7	74.6	78	2	20
S10	1210	949	48600	35600	42000	212	160000	60.8	997	7.3	76.9	87.2	3.8	9
Mean	1025.8	903.7	48030	39780	47440	362.2	138580	58.78	902.3	8.0	79.9	-	-	-
St. dev.	606.4	108.2	5567.2	14098	13099	275.4	37505	14.6	319.2	2.2	15.2	-	-	-
Coeff. Of variation	59.1	11.9	11.6	35.4	27.6	76.03	27.1	24.9	35.4	27.2	19.0	-	-	-

Table 2 — Correlation matrix of heavy and major elements of soil samples

	Cr	Mn	Fe	Al	Ca	P	Mg	Co	Ni	Pb	Zn	Clay	Silt	Sand
Cr	1													
Mn	−0.29	1												
Fe	0.09	0.51	1											
Al	0.15	0.64	0.36	1										
Ca	0.04	−0.02	0.12	0.63	1									
P	−0.41	0.80**	0.36	0.80*	0.18	1								
Mg	0.47	−0.73*	−0.41	−0.93**	−0.54	−0.82**	1							
Co	0.21	−0.75*	−0.40	−0.98**	−0.57	−0.79**	0.95**	1						
Ni	0.34	−0.76*	−0.42	−0.97**	−0.55	−0.81**	0.98**	0.99**	1					
Pb	−0.03	0.31	0.14	0.84**	0.73*	0.76*	−0.84**	−0.80**	−0.80**	1				
Zn	−0.24	0.51	0.70*	0.72*	0.48	0.71*	−0.76*	−0.71*	−0.74*	0.73*	1			
Clay	−0.75*	0.40	−0.33	0.29	0.03	0.48	−0.46	−0.36	−0.43	0.28	0.10	1		
Silt	0.04	−0.06	0.10	−0.37	−0.11	−0.25	0.14	0.14	0.16	−0.53	−0.42	−0.30	1	
Sand	0.70*	−0.36	0.26	−0.05	0.04	−0.33	0.37	0.27	0.33	0.07	0.17	−0.80**	−0.33	1

*Correlation is significant at the 0.05

**Correlation is significant at the 0.01

environments are well intercorrelated. The elements Al, P, Pb, and Zn are well correlated with each other showing poor abundance of these elements in ophiolitic regions. Cr, which is geochemically categorized in the first group, also shows good correlation, but its relation is not as strong as those elements. There is an intense negative correlation among Al, Mg, Ni, and Co. These relationships seem to be rational, as Al predominately occurs in acidic rocks. The similar correlations are also observed among Pb, P, and Zn with the mentioned elements.

The relations of the studied elements with percentage of clay and sand content of soil samples are categorized into three groups: 1- Elements have a better relationship with sand fraction, e.g., Cr, Ni, Fe, Mg, and Co. 2- Elements have a better relationship with clay fraction, e.g., Al, P, Mn, and Pb. 3- Elements do not show any considerable relationship with soil texture, e.g., Zn and Ca.

Coarse-grained materials probably showing the presence of parent materials; thus, elements in the first group are dominantly distributed via coarse grains weathered from ultramafic rocks than adsorbed on clay minerals. Elements in group 2 are placed in silicate layers easily, and with increase of clay content, their concentration increases. Given this, the sorption and desorption processes play a more important role in transportation of these elements in soils of the study area.

A soil is considered "clean" when the substance under environmental concern occurs in concentrations equal or lower than the value found in nature, which is used as reference and usually named background concentration. Table 3 shows the background concentrations for different elements in some international standards. Comparing the metal and major elements of the soil samples with those of standards shows that concentrations of the elements Cr, Mn, Mg, Co, Ni, and Zn for most of the soil samples were above permissible levels.

To identify the natural enrichment of most common elements in the study area, enrichment factor was calculated according to:

$$EF = {}^{(C/R)\ \text{sample}}/_{(C/R)\ \text{crust}}$$

Where EF is the enrichment factor, *C* is the concentration in soil or earth crust, and *R* is the reference element concentration (normalizing element). Sc was used as the reference element. Crust concentrations were adopted from Rudnick and Gao[19]. Enrichment factor greater than 1 indicates that the metal is more abundant in the soil relative to earth crust in the regional background. The calculated enrichment factors for elements Cr, Mn, Co, Ni, Pb, Zn, and P in 10 soil samples of the study area are shown in Fig. 3.

Another index that has been used to assess the degree of contamination of soil samples is geoaccumulation index [23]. The index is calculated as: Igeo=Log2(Cn/1.5Bn).

Where Igeo is the geoaccumulation index, Log_2 is log base 2, C_n is the concentration in soil or sediment, and B_n is the background or reference concentration. Similar to the enrichment factor, the reference values adopted were the average concentration of elements in

Table 3 — Limits for heavy metals and major elements in soils (mg/kg)

Standard	Co	Cr	Mg	Mn	Ni	P	Pb	Zn
Lindsay[20]	8	10	5000	600	40	600	10	50
USEPA[21]	8	10	5000	600	40	600	10	50
UK[22]	-	50	-	-	50	-	100	300
Australiac	-	100	-	-	100	-	100	300

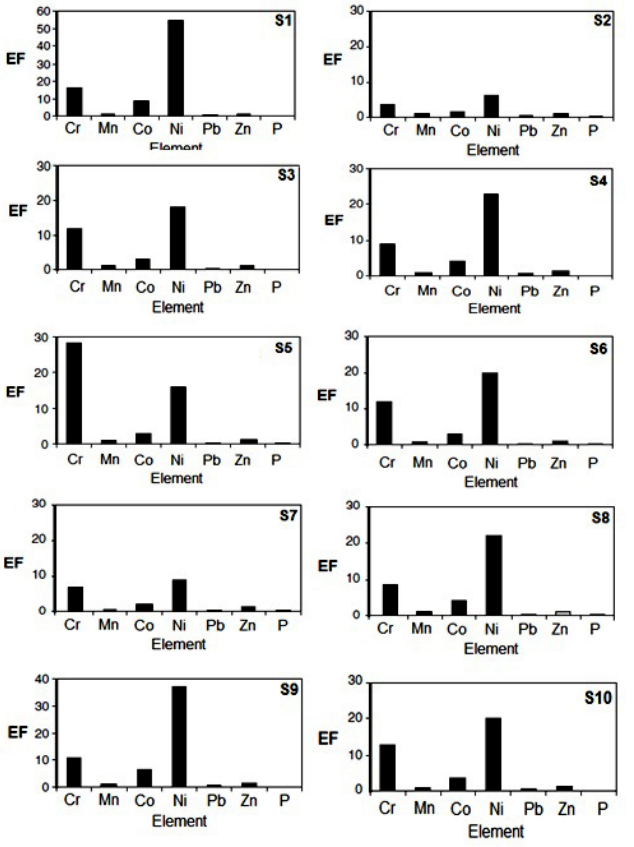

Fig. 3 — Calculated enrichment factor for the studied elements in Harsin-Sahneh region.

the earth's crust estimated by Rudnick and Gao [19]. Muller [31] classified soils in terms of quality (Table 4). Based on this index, Table 5 shows calculated geoaccumulation. As can be seen from this table, few heavy metals like Cr, Ni, and Co have values above zero, and hence, degree of contamination in thes heavy metals is a matter of consideration.

In Harsin–Sahneh region as respects main lihology consists of mafic and ultramafic rocks; therefore, to perception the origin of soil contamination and determination of magma characteristic we do geochemical studies and systematically compared the variation of major and trace element of selected samples. The geochemical features of the rocks studied in this paper are described using major and trace elements that are virtually immobile during low-temperature alteration and metamorphism.

According on electron probe micro-analysis results, the mean of structural formula for olivine calculated based on four oxygen atoms ($Mg_{1.65}$, $Fe^{2+}_{0.35}$ $Ti_{0.01}$) ($Si_{0.97}$ $O_{3.98}$). In the Fe^{2+}/ (Fe^{2+}+ Mg) *versus* Mg/ (Fe^{2+}+ Mg) diagram, all of the olivine fall in the chrysolite field (Fig.4a). The average composition for three samples of olivine in the Harsin gabbro with a structural formula is reported in Table 6. Plagioclases have a quite restricted compositional range (anorthite = 56.5–64.6%).

Based on electron probe micro-analysis results, the mean of structural formula for plagioclases was calculated based on 32 oxygen atoms ($Ca_{0.63}$, $Na_{0.41}$, $K_{0.01}$) ($Si_{2.35}$ $Al_{1.61}$ $O_{8.05}$). In Or-Ab-An trilateral diagram, all of the plagioclases fall in the labradorite field (Fig. 4b). Table 6 shows the mean of the three samples of plagioclase in the Harsin gabbro with structural formula.

Pyroxene compositional ranges are SiO_2 (48.3–51.9%), MgO (15.4–18.7%), and TiO_2 (0.15–3.31%). All of the pyroxene crystals are rich in Ca (Wo = 34–48 wt. %) and poor in Na (Na_2O <0.58 wt. %). Pyroxene compositional ranges vary from En_{45} Fs_6 Wo_{34} to En_{54} Fs_{12} Wo_{48}; besides in pyroxene trilateral diagram (enstatite, ferrosilite, wollastonite), all of the samples are placed in the diopsidic augite field (Fig. 4c).

Based on electron probe micro-analysis results, the mean of structural formula for clinopyroxenes was calculated based on six oxygen atoms ($Ca_{0.86}$, $Na_{0.04}$, $Mg_{0.86}$, Fe^{2+} $_{0.13}$, $Ti_{0.04}$) ($Si_{1.83}$ $Al_{0.15}$ $O_{5.94}$). Table 6 presents the mean of the three samples of pyroxene in the gabbros with structural formula.

The plot of analysis results in FeO_{total}/MgO *versus* SiO_2 diagram and AFM trilateral diagram indicate that all samples fall in calc-alkaline field (not show). Based on major and trace element geochemical data (Table 7), Harsin gabbro samples have a compositional range SiO_2 (47/40–50/50 %), Al_2O_3 (16/50–23/0 %), Fe_2O_3 (5/16–3/76 %), MgO (9/21–12/25 %), MnO (0/07– 0/08 %), P_2O_5 (less than 0/01% in all samples), and TiO_2 (0/27 -0/06%). Sr, Co, Ni, and V contents are relatively high, whereas other element contents relatively low.

Generally, low TiO_2 content predicts the deficiency of oxide in parental gabbroic magma. According to Pearce and Norry [24], the low Ti content reflects the degree of depletion of the mantle source. Therefore, in the Harsin gabbro samples, low TiO_2 content reflects the removal of TiO_2 during previous partial melting events and crystallization from primary magmas generated from mantle sources undergoing earlier partial melting. In the gabbro samples, Ni and

Table 4 — Igeo classes and sediment quality (after Muller [23])

Igeo	Soil quality
< 0	Unpolluted
0–1	Unpolluted to moderately polluted
1–2	Moderately polluted
2–3	Moderately to highly polluted
3–4	Highly polluted
4–5	Highly to very highly polluted
5–6	Very highly polluted

Table 5 — Calculated Igeo for soil samples of study area

Element	Soil samples									
	S1	S2	S3	S4	S5	S6	S7	S8	S9	S10
Cr	2.61	1.66	2.97	2.38	4.24	3.12	2.57	2.26	2.32	3.13
Mn	−0.87	−0.45	−0.86	−0.90	−0.66	−0.77	−0.63	−0.59	−1.02	−0.66
Co	1.72	0.46	1.03	1.21	1.05	1.21	0.70	1.19	1.57	1.23
Ni	4.38	2.30	3.58	3.70	3.41	3.84	2.96	3.67	4.14	3.82
Pb	−2.27	−1.03	−1.69	−1.62	−1.91	−1.82	−1.20	−1.89	−1.93	−1.80
Zn	−0.64	−0.10	−0.47	−0.48	−0.06	−0.48	0.14	−0.62	−0.43	−0.39
P	−4.05	−1.37	−3.53	−3.82	−3.07	−2.50	−1.45	−2.38	−4.11	−3.41

Table 6 — Chemical composition of olivines, plagioclase and pyroxene of Harsin gabbro

Sample name	B7	B13	B22	B7	B13	B22	B7	B13	B22
Point	2	9	6	7	8	8	10	4	3
Mineral		Olivine			Plagioclase			Pyroxene	
Oxides		4 oxygen			32 oxygen			6 oxygen	
SiO_2	37.55	38.96	37.00	51.12	50.68	51.66	50.67	50.09	50.36
TiO_2	1.03	0.10	0.75	0.23	0.69	0.41	0.96	1.40	0.88
Al_2O_3	0.02	0.02	0.03	29.29	30.06	30.06	2.82	4.04	3.72
FeO	16.68	17.15	16.68	0.59	0.10	0.06	6.01	5.00	4.41
MnO	0.27	0.00	0.07	0. 11	0.00	0.00	0.05	0.00	0.00
MgO	43.42	42.55	44.47	0.01	0.02	0.02	17.61	17.12	16.27
CaO	0.05	0.04	0.05	12.69	12.73	12.80	20.70	21.22	23.17
Na_2O	0.08	0.05	0.03	4.61	4.60	4.54	0.45	0.56	0.53
K_2O	0.03	0.02	0.01	0.18	0.04	0.15	0.02	0.01	0.01
Total	99.12	98.89	99.08	98.83	98.89	99.69	99.28	99.42	99.34
Si	0.96	1.00	0.95	2.36	2.34	2.36	1.86	1.81	1.84
Al	0.00	0.00	0.00	1.59	1.63	1.61	0.12	0.18	0.15
T-site	0.96	1.00	0.95	3.96	3.97	3.97	1.98	1.98	1.99
Al	-	-	-	-	-	-	0.00	0.00	0.01
Ti	0.02	0.00	0.01	0.01	0.02	0.01	0.03	0.05	0.02
Fe^{2+}	0.35	0.37	0.35	0.02	0.00	0.00	0.18	0.16	0.13
Mn	0.01	0.00	0.00	0.00	0.00	0.00	0.00	0.00	0.00
Mg	1.65	1.63	1.65	0.00	0.00	0.00	0.96	0.92	0.90
Ca	0.00	0.00	0.00	0.63	0. 63	0. 62	0.81	0.85	0.92
Na	0.00	0.00	0.00	0.41	0.41	0.42	0.03	0.04	0.04
K	0.00	0.00	0.00	0.01	0.00	0.01	0.00	0.00	0.00
Cations	2.05	2.00	2.07	-	-	-	-	-	-
Mg/Fe+Mg	0.83	0.82	0.83	-	-	-	-	-	-
X site	-	-	-	1.08	1.04	1.04	-	-	-
M-site	-	-	-	-	-	-	1.08	1.04	1.04
Ab	-	-	-	39.26	39.29	38.76	-	-	-
An	-	-	-	59.76	60.49	60.39	-	-	-
Or	-	-	-	1.01	0.24	0.89	-	-	-
Wo	-	-	-	-	-	-	41.39	44.0	47.30
En	-	-	-	-	-	-	49.22	47.91	46.22
Fs	-	-	-	-	-	-	9.40	3.09	6.48

Cr contents are also relatively high, ranging from 126 to 358 ppm and from 68 to 958 ppm, respectively, and SiO_2 content ranging from 47/43 to 50/50 wt. %. Ni and Cr contents reject the claim that these rocks are generated from primary magma, which could occur due to petrogenetic process (such as differentiation) or inherited from metasomatised mantle sources.

Parlak et al.[25] suggested that primary clinopyroxenes that crystallized from basic magma in low-pressure condition usually have Mg number less than 84; Mg number of clinopyroxenes in our samples is between 82 and 87; therefore, clinopyroxenes in the Harsin gabbros formed at a low-pressure condition. Low anorthite content in Harsin gabbro plagioclases (An_{56}–An_{64}) is commonly related to the crystallization of calcic plagioclase in the early stages of magma differentiation.

In F1 *versus* F2 diagram [26] which is based on the composition of major and trace element of clinopyroxenes for the discrimination of basalt tectonic setting; clinopyroxenes of Harsin gabbros falls in the Volcanic Arc Basalt (VAB) field (Fig. 4d); moreover, plot of the results in TiO_2-Y/20-K_2O diagram [27] prove that Harsin gabbros fall in the same field (not show).

Likewise, the analysis findings of mafic and ultramafic samples of Sahneh region (Table 8) placed in several diagrams. In the total alkali (Na_2O + K_2O) *versus* SiO_2 diagram (Fig. 4e) the gabbroic samples are placed in the sub-alkaline field. In the AFM diagram (Fig. 4f) samples fall in the tholeiitic domain. To find more details about tholeiitic magma, the Jensen diagram [28] was used. Plot of the

Table 7 — ICP-AES and ICP-MS analyses of selected representative rocks (Harsin gabbro)

sample	B10	B12	B14	B19	B23	B05	B07	B09	B13	B22
SiO_2	49.46	48.40	49.80	50.50	49.61	49.10	50.25	47.43	18.15	48.20
TiO_2	0.26	0.19	0.24	0.25	0.19	0.24	0.27	0.12	0.11	0.06
Al_2O_3	18.78	17.58	18.20	16.50	20.38	18.50	17.58	21.65	21.76	23.03
Fe_2O_3	1.80	1.67	1.74	1.75	1.72	1.74	1.80	1.59	1.59	1.56
FeO	2.64	3.12	3.12	2.70	2.29	2.48	2.51	3.30	3.50	2.20
MnO	0.08	0.08	0.08	0.08	0.07	0.07	0.07	0.08	0.08	0.05
MgO	9.21	12.25	9.85	11.20	7.82	9.78	9.67	10.92	10.36	8.65
CaO	14.57	13.73	12.90	13.70	13.35	13.60	13.89	11.51	10.83	10.60
Na_2O	2.36	1.96	2.70	2.30	2.57	2.60	2.66	2.46	2.86	3.10
K_2O	0.08	0.08	0.03	0.01	0.05	0.1	0.1	0.1	0.02	0.01
P_2O_5	0.01	0.01	0.01	0.01	0.01	0.01	0.01	0.01	0.01	0.01
LOI	0.53	0.75	0.76	0.86	1.66	1	0.56	0.76	0.74	0.41
Total	99.78	99.83	99.43	99.93	99.91	99.22	99.35	99.92	99.98	99.96
U	0.97	0.27	0.05	0.05	0.05	0.05	0.83	0.52	1.36	0.58
W	1	1	1	1	1	1	1	1	1	1
Sn	1	1	1	1	1	1	1	1	1	1
Ba	20	20	10	20	10	20	20	30	10	20
Rb	2.6	0.08	1.2	0.3	0.2	0.5	1.1	0.5	0.2	0.04
Sr	280	280	180	200	250	270	230	310	200	310
Zr	8.2	6.8	5.9	7.5	4.5	6.6	7.4	2.6	2	1.3
Nb	1	1	1	1	1	1	1	1	1	1
Th	0.9	0.5	0.2	0.2	0.1	0.1	0.5	0.5	0.7	0.6
Ga	12	11	11	11	12	10	11	12	12	13
Zn	24	32	33	30	18	29	17	32	29	22
Cu	56	91	89	60	39	59	70	51	60	13
Ni	126	238	162	183	174	239	176	358	209	226
V	93	96	109	105	71	96	148	47	36	22
Cr	958	684	205	274	479	616	78	753	432	274
Hf	1	1	1	1	1	1	1	1	1	1
Cs	0.2	0.1	0.1	0.1	0.1	0.1	0.1	0.1	0.1	0.1
Ta	0.5	0.5	0.5	0.5	0.5	0.5	0.5	0.5	0.5	0.5
Co	29.8	41.6	33	31.2	23.4	30.4	29.1	41	39.7	29.9
Y	8.3	6.8	6.7	7.4	5.1	5.9	8.5	3.2	2.9	1.6
La	3.4	2.4	1.9	1.4	0.8	1.3	2.4	2.4	1.8	3.8
Ce	4	3.1	1.2	1.5	0.7	1.6	2.8	2.7	1.4	1.7
Pr	0.69	0.49	0.39	0.37	0.22	0.39	0.50	0.41	0.29	0.27
Nd	3.5	2.5	1.8	1.9	1.3	2	2.7	1.8	1.2	1.1
Sm	0.9	0.7	0.6	0.6	0.5	0.7	0.9	0.5	0.3	0.2
Eu	0.52	0.45	0.48	0.43	0.40	0.52	0.61	0.42	0.35	0.29
Gd	1.3	1.5	0.88	0.95	0.79	1	1.38	0.56	0.43	0.18
Tb	0.22	0.17	0.17	0.18	0.11	0.17	0.22	8.07	0.07	0.05
Dy	1.44	1.11	1.15	1.23	0.83	1.06	1.48	0.54	0.44	0.23
Ho	0.31	0.24	0.21	0.23	0.16	0.21	0.28	0.12	0.1	0.05
Er	0.87	0.72	0.63	0.76	0.51	0.58	0.82	0.29	0.26	0.12
Tm	0.12	0.10	0.09	0.10	0.07	0.09	0.12	0.05	0.05	0.05
Yb	0.7	0.05	0.05	0.6	0.4	0.5	0.8	0.3	0.2	0.1
Lu	0.09	0.08	0.08	0.08	0.05	0.08	0.12	0.05	0.05	0.05
Mg #	0.89	0.86	0.86	0.88	0.89	0.86	0.87	0.86	0.80	0.68

findings in the diagram indicate that parent magma in gabbroic sequence is a high Mg tholeiitic magma (HMT— Fig. 4g). The Cr *versus* Ti diagram shows that the composer magma from Sahneh is rich in MgO while little in K_2O. Microscopic and geochemical evidences indicate that not only is olivine of these rocks forstrite in nature, but NiO content also is somewhat related to the forstrite contents. Moreover, high NiO content in Sahneh samples indicate that the olivine (with high

Table 8 — XRF analyses results of selected gabbros and pridotites rocks of Sahneh region

Rock	Gabbro								Pridotite					
Oxides	MX-1	K-5	D-4	D-5	MS-3	K-4	C-1	G-1	P-9	MD-3	P-1	H-2	P-5	H-1
SiO_2	50.66	49.47	47.56	48.71	40.27	54.09	47.48	51.67	35.51	34.23	36.45	36.5	53.8	35.86
TiO_2	14.66	16.39	17.53	13.34	22.46	21.04	17.99	12.73	5	4.63	5.69	4.7	5.46	5.11
Al_2O_3	1.94	1.64	1.9	1.69	1.5	1.96	2.15	2.07	1.5	1.51	1.53	1.51	0.66	1.5
Fe_2O_3	3.32	2.67	3.8	7.7	1.46	2.2	8.06	6.17	7.79	8.78	8.19	8.12	0	9.29
FeO	11.75	12.29	12.75	13.44	16.18	4.68	10.05	9.31	48.69	49.51	45.01	47.42	29.6	44.95
MnO	12.16	14.98	13.06	10.97	16.29	10.63	9.52	12.81	1.15	0.49	1.79	0.73	9.89	1.03
MgO	3.47	1.12	2.07	2.74	0.45	2.79	2.52	3.05	0.04	0.05	0.21	0.05	0.3	0.08
CaO	0.05	0.04	0.22	0.06	0	0.11	0.91	0.02	0	0.01	0.15	0	0.02	0.01
Na_2O	0.12	0.11	0.14	0.18	0.02	0.01	0.17	0.14	0.12	0.13	0.13	0.12	0.01	0.13
K_2O	0.44	0.14	0.4	0.19	0	0.46	0.65	0.57	0	0.01	0.03	0.01	0	0
P_2O_5	0.02	0	0.02	0.04	0.01	0.01	0.05	0.04	0.01	0.01	0.01	0.01	0.01	0.01
Cs	23	29	20	22	20	24	19	23	-	-	-	-	-	-
Ga	13	11	12	13	12	14	13	10	1	4	5	2	1	4
Mo	2	1	2	2	1	2	1	2	-	-	-	-	-	-
Sn	4	4	4	4	5	5	4	5	-	-	-	-	-	-
Th	1	4	3	1	4	2	3	3	-	-	-	-	-	-
Ni	155	289	189	215	120	140	77	78	2850	3213	2628	3004	1433	2901
Rb	1	1	1	1	2	2	4	1	-	-	-	-	-	-
Sr	101	141	154	101	150	155	686	41	5	8	10	12	1	12
Y	18	10	8	17	12	10	23	15	2	4	4	2	3	4
Cr	71	836	633	719	520	560	312	128	117	112	100	122	141	127
Zr	45	49	52	51	50	58	95	46	-	-	-	-	-	-
Nb	3	2	2	1	3	1	1	7	-	-	-	-	-	-
Ba	408	410	412	398	395	351	400	403	22	22	22	22	22	22
La	13	14	13	11	12	13	13	13	1	0	0	1	0	0
Ce	11	11	11	11	11	11	18	11	-	-	-	-	-	-
Nd	0	1	4	2	5	3	6	6	-	-	-	-	-	-
Sm	0	3	1	3	2	2	1	2	1	0	1	0	1	0
Yb	2	2	2	2	2	2	2	2	-	-	-	-	-	-
Eu	1	1	1	1	1	1	2	1	1	1	1	1	1	1
Sc	32	35	33	30	29	28	28	31	3	1	5	4	8	4
V	180	177	176	193	180	198	190	187	21	4	25	9	21	15
Pb	8	4	6	3	5	4	5	8	3	4	4	4	4	4
Cu	118	87	45	35	38	36	123	78	8	5	26	2	47	50
Co	50	51	50	47	53	50	47	48	122	131	131	122	76	128
Zn	25	22	14	13	20	17	42	11	68	68	70	66	63	69
Total	98.66	99.11	99.45	99.28	98.64	98.98	99.55	98.11	99.81	99.36	99.19	99.17	99.75	99.97

NiO content) is crystallized from relatively primitive magmas.

Studing Sahneh gabbro in Al_2O_3 , FeO, and MgO diagram to determine paleotectonic setting (Fig. 4h) and V *versus* Ti diagram (not show) proved that samples fall in the mid-ocean ridge basalt (MORB) field. In order to clarify the nature of the environment of basalts (MORB), analyze results plotted in Zr-Nb-Y diagram. This plot indicates that the samples were located in the MORB field is likely from the E-MORB environment (Fig. 4i).

Thus, selected minor and trace elements (e.g. Ti, Zr, Y, and Nb) are used to characterize such basalts with respect to the original composition and possible tectonic environment of formation, for these elements are believed to be relatively immobile under conditions of alteration and low-grade hydrothermal metamorphism.

The incompatible element pattern of the Harsin gabbro (Fig. 4j) indicates both negative anomalies in Zr, Nb, and Ce and positive in Sr and La anomalies for samples. These incompatible element patterns are characterized by an overall negative slope (generally sloping downward to the right). Positive anomalies in Sr are characteristic of rocks that have high modal concentrations of calcic plagioclase. As a matter of fact, both negative anomalies in Nb, Ti, Hf, and Zr and positive anomalies in U are considered to be a

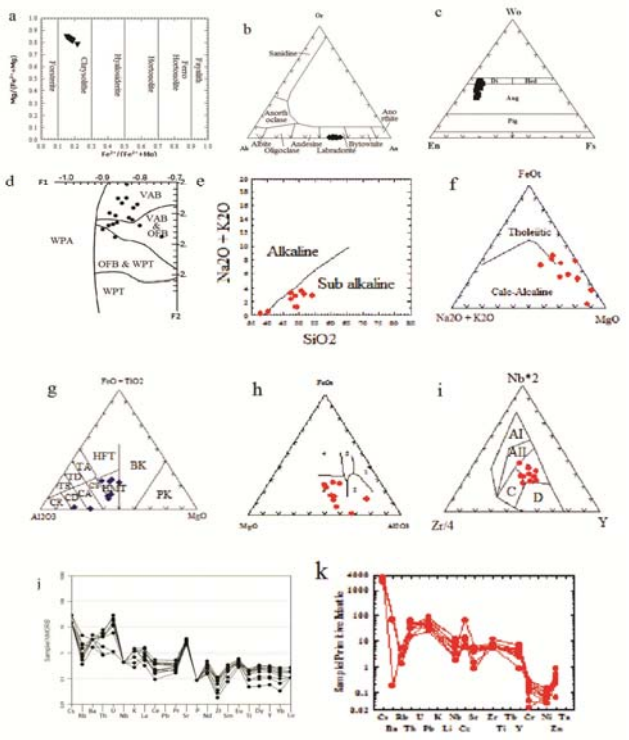

Fig. 4 — Plot of analysis result in different diagrams. a. Olivine composition in Mg/(Fe^{2+} + Mg) versus Fe^{2+}/(Fe^{2+} + Mg) diagram for gabbro rocks of the Harsin (Deer et al.[29]). b. Plagioclases composition in Or-Ab-An trilateral diagram for gabbro rocks of the Harsin (Shelley [30]). c. Pyroxenes composition in Or-Ab-An trilateral diagram for gabbro rocks of the Harsin (Morimoto et al. [31]). d. F1–F2 diagram for clinopyroxene of gabbro rocks of the Harsin. e. $Na_2O + K_2O$ versus SiO_2 diagram for ultramafic and mafic rocks of the Sahneh. f. AFM diagram for ultramafic and mafic rocks of the Sahneh.g. Jensen [39] diagram for ultramafic and mafic rocks of the Sahneh. h. Al_2O_3, FeO_t, and MgO diagram for ultramafic and mafic rocks of the Sahneh. i. Nb-Zr-Y geochemical discrimination diagram for ultramafic and mafic rocks of the Sahneh (Meschede [32]). j. Incompatible element patterns of mafic rocks of Harsin normalized to MORB Sun and McDonough's [33]. k. Incompatible element patterns of ultramafic and mafic rocks of the Sahneh normalized to primitive mantle Sun and McDonough's [33].

signature of a mantle source over a subduction zone. Most likely, they were derived from a depleted mantle which was slightly metasomatised over a subduction zone.

The rare earth element (REE) patterns for the mantle rocks of Sahneh region show depletion in the light REE (LREE) but enrichment in heavy REE (HREE) (Fig. 4k). These patterns are similar to the E-MORB-type tholeiites; based on the evidence of the normalized incompatible trace element diagram and the discrimination plots, it is concluded that Sahneh basalts were derived from melts generated in the E-MORB environment.

Discussion

Based on analyses results of soils samples were collected from the study area, the obtained results show that most of heavy and major elements were exceeding the permissible levels in soil samples in the study area. The main reason for such enrichment would be the presence of ultramafic rocks and weathering and leaching of elements from them. Therefore, natural contamination and morphology play important roles in producing such a high concentration of heavy metals in a region.

Most of the soil samples are below the standard limits for P and Pb. The low concentration of these two elements is due to a low concentration of these elements in ultramafic rocks.

Based on EF factor most elements in most samples are enriched compared to those in earth crust. Cr and Ni are by far more enriched than other elements in this area (Fig. 3). After these two heavy metals, Co is slightly more enriched comparing with others. Pb and P had an EF lower than 1, showing that the contents of these elements in topsoils are lower than those in earth crust. The higher enrichment of heavy and toxic

metals Cr, Ni, and Co is due to development of soil in ultramafic environments.

The Igeo values in some elements (e.g. Mn, Pb, Zn, and P) are below zero, but in chromium content, 80% of the soil samples are moderately to highly polluted, ten percent are highly polluted, and 10% are moderately polluted. Ni has a similar condition. Sixty percent of the soil samples are moderately to highly polluted. Co is another abundant element in ultramafic environments, which their contamination degree is classified as moderately polluted; other samples are uncontaminated (Table 5).

Ophiolites in Zagros orogenic belt are keys for reconstructing the Neo-Tethyan realm from rifting to the beginning of collision. Studies of the ophiolite complexes in Zagros orogen indicate that most of Zagros ophiolites were generated in an intra-oceanic island arc environment. These studies suggested that during intra-oceanic subduction, an immature island arc developed before ocean closure.Subduction slab collapsed during this phase mostly led to the large-scale extension of overriding oceanic plate and thereby to the generation of suprasubduction ophiolites.

Tectonic events lead to the formation of Kermanshah arc to occur as follows: Sanandaj–Sirjan continental arc magmatism had ended in the Late

Cretaceous. It may be that the Southern Neo Tethyan oceanic crust broke into the Late Cretaceous, subdued beneath itself, and developed arc magmatism in Kermanshah region. As a result, Neo-Tethyan oceanic crust subduction beneath the SSZ stopped at this time.

Therefore, in the Late Cretaceous, arc magmatic-related rocks developed in Kermanshah ophiolites. All of mafic and ultramafic rocks in Harsin Sahneh ophiolites are resting on the top of Neo-Tethyan slab under Eurasia. Sedimentary age constraints in Kamyaran region (NW Kermanshah) and North of Harsin–Sahneh, along the Gamasiab River, indicate that the subduction-related magmatism has been active mainly between the Paleocene and the Eocene [10].

Paleocene to Eocene magmatism quiescent period spanning in SSZ roughly coincides with arc-related magmatism in Kermanshah region. By the end of short-live magmatism in Kermanshah, continental arc magmatism resumed in Middle Eocene onwards along Urumieh– Dokhtar arc, which caused an inland shift around 200 km (shift from the Sanandaj–Sirjan arc to the Urumieh–Dokhtar arc).

Based on evidence, Harsin–Sahneh ophiolites were a magmatic arc built on the Neo- Tethyan oceanic lithosphere at the distal part of Eurasian margin, but MORB-related magmatism occurred in response to the reduction of convergence rate of Neo-Tethyan. During the Paleocene–Eocene, the rate of convergence of Eurasian continental margin slowed down; this reduction may have subdued slab retreat, triggering the development of back-arc extension at Eurasian margin. This would also explain the simultaneous occurrence of MORB-type and arc-type magmatism.

Moreover, other evidence indicates that basaltic rock assemblage in Harsin–Sahneh ophiolites occurred in different tectonic environments. LREE and HREE patterns show that different mixing occurred in the asthenospheric sources. All previous studies in recent years proved that Kermanshah ophiolites represent a particular case of an ophiolitic sequence.

Conclusion

Soil texture studies suggest that the concentrations of Cr, Ni, Fe, Mg, and Co, which are more abundant in ultramafic environments, are well correlated with sand fraction of soil samples, while the concentrations of Al, P, Mn, and Pb are positively correlated with clay percentage of soil. Such a finding suggests that mainly ultramafic-originated elements are transported in coarse grain particles specifically via physical factors. Heavy and major elements of soil samples are above permissible levels of the Environmental Protection Agency, UK, Australia, and Lindsay for Cr, Mn, Mg, Co and Zn. Calculated EF for soil samples are significant for Cr and Ni. Geoaccumulation factor index also showed which of the elements Cr, Ni, and Co are among the most contaminating metals of soil samples in the study area. In addition, textural and chemical data suggest that Harsin–Sahneh ophiolites in West of Iran recorded geodynamic evolution of Southern Neo-Tethys Ocean. Geochemical signatures show that Harsin–Sahneh ophiolites are related to oceanic intra plate arc tectonic setting. Studies in recent years indicate that oceanic components abducted over the Arabic–Tauric platform during the Late Eocene to Early Oligocene, which is considered as the final closure of Southern Neo- Tethyan and Iran–Eurasia collision. In the Late Cretaceous, the subduction of Southern Neo-Tethyan Ocean beneath itself leads to the cessation of subduction beneath the SSZ; therefore, at this time, Sanandaj–Sirjan continental arc magmatism had ended and arc magmatism activity developed in the Kermanshah region. Radiometric age indicates that the quiescent period of magmatism in SSZ roughly coincides with arc-related magmatism in the Kermanshah region. The resumption of subduction in region leads to forming arc-, back-arc-, and E-MORB-related rocks in Sahneh–Harsin regions and Sonqor–Baneh and Hamedan–Tabriz volcanic belts. The reduction in the rate of convergence and slab retreat subduction had back-arc extended in the Eurasian margin; this could be considered as a factor in mixed MORB and arc geochemical signatures of Kermanshah magmatism. The secondary stage of magmatism occurred after Kermanshah ophiolite abduction; in this stage, magmatism activity shifted from Sanandaj–Sirjan arc to the Urumieh–Dokhtar arc.

Acknowledgment

The authors wish to thank the Journal Manager and reviewers who critically reviewed the manuscript and made valuable suggestions for its improvement.

References

1 Azizi, H. and Moinevaziri, H., Review of the tectonic setting of Cretaceous to Quaternary volcanism in northwestern Iran, *Geodynamic Journal*, 47 (2009) 167-179.

2 Fazlnia, A.N., Moradian, A., Rezaei, K., Moazzen, M. and Alipour, S., Synchronous activity of anorthositic and S-type granitic magmas in the Chah-Dozdan batholith,Neyriz, Iran: evidence of zircon SHRIMP and monazite CHIME dating, *Journal of Sciences*, *Islamic Republic of Iran,* 18 (2007) 221-237.

3 Shahabpour, J., Tectonic evolution of the orogenic belt in the region located between Kerman and Neyriz, *J. Asian Earth Sci.,* 24 (2005) 405-417.

4 Ventura, F., Salvatorelli, F., Piana, S., Pieri, L. and Pisa, P., The effects of biochar on the physical properties of bare soil, *Earth and Environmental Science Transactions of the Royal Society of Edinburg,* 103 (2012) 5-11.

5 Zarei Sahamieh, R., Moradpour, A., Geochemistry and petrology of Harsin–Sahneh ophiolitic complex (NE of Kermanshah—west of Iran) an evidence of Southern Neo-Tethys Ocean tectonic, *Arab J Geosci*, 8 (2015) 8347-8360.

6 Moradpour, A., Zarei Sahamieh, R., Ahmadi Khlaji, A. and Sarikhani, R., Textural records and geochemistry of the Kermanshah mantle peridotites (Iran): implications for the tectonic evolution of southern Neo-Tethys , *J. of Geosci*, 62 (2017) 165-186.

7 Miati, S., Gupta, G., Erram, V. and Tiwari, R., Delineation of shallow resistivity structure around Malvan, Konkan region, Maharashtra by neural network inversion using vertical elecrtical sounding measurments, *Environ Earth Sci*, 68 (2013) 779-794.

8 Braud, J., La suture du Zagros au niveau de Kermanshah (Kurdistan iranien): reconstitution paléogéographique, *évolution géodynamique, magmatique et structurale*, Université Paris-Sud, (1987) 450 pp.

9 Ricou, L.E., Braud, J. and Brunn, J.H., Le Zagros. Livre à la mémoire de A.F. de Lapparent (1905–1975). *Mémoire hors Série de la Société Géologique de France*, 8 (1977) 33-52.

10 Gharib, F., Biostratigraphy des radiolarites de Kermanshah (Iran). Unpublished doctoral dissertation, *Museum Nationald'Histoire Naturelle (Paris)*, 2009 343 pp.

11 Ricou, L.E., Le croissant ophiolitique péri-arabe, une ceinture de nappes mise en place au crétacé supérieur. *Revue de Géographie Physique et de Géologie Dynamique*, 18 (1971) 327-350.

12 Delaloye, M. and Desmons, J., Ophiolites andmelange terranes in Iran: a geochronological study and its paleotectonic implications. *Tectonophysics*, 68 (1980) 83-111.

13 Whitechurch, H., Omrani, J., Agard, P., Humbert, F., Montigny, R. and Jolivet, L., Evidence for Paleocene–Eocene evolution of the foot of the Eurasian margin (Kermanshah ophiolite, SWIran) from back-arc to arc: Implications for regional geodynamics and obduction, *Lithos*, 182-183 (2013) 11-32.

14 Wrobel-Daveau, J.C., Ringenbach, J.C., Tavakoli, S., Ruiz, G., Masse, P. and Frizonde Lamotte, D., Evidence for mantle exhumation along the Arabian margin in the Zagros (Kermanshah area, Iran). *Arabian Journal of Geosciences*, 3 (2010) 499-513.

15 Saccani, E., Allahyari, K., Beccaluva, L. and Bianchini, G., Geochemistry and petrology of the Kermanshah ophiolites (Iran): implication for the interaction between passive rifting, oceanic accretion, and OIB-type components in the Southern Neo-Tethys Ocean, *Gondwana Res*, 24 (2013), 392-411.

16 Allahyari, K., Saccani, E., Rahimzadeh, B. and Zeda, O., Mineral chemistry and petrology of highly magnesian ultramafic cumulates from the Sarve-Abad (Sawlava) ophiolites (Kurdistan, NW Iran): New evidence for boninitic magmatism in intra-oceanic fore-arc setting in the Neo-Tethys between Arabia and Iran, *J. Asian Earth Sci.,* 79 (2014) 312-328.

17 Nicolas, A., Boudier, F. and Bouchez, J.L., Interpretation of peridotite structures from ophiolitic and oceanic environments, *Am. J. Sci.*, 28 (1980) 192-210.

18 Tukey, J. W., Exploratory data analysis. Reading7: *Addison-Wesley* (1977).

19 Rudnick, R. L. and Gao, S., The composition of the Continental Crust (pp. 1–64). In R. L. Rudnick (Ed.), The Crust (Vol. 3), H. D. Holland & K. K. Turekian (Eds.), *Treatise on geochemistry*. Oxford: Elsevier- Pergamon, (2003).

20 Lindsay, W. L., Chemical equilibria in soils , New York: *Wiley*, (1979) 449 pp.

21 USEPA ,Office of Solid Waste and Emergency Response, *Hazardous waste land treatment*, SW-874 (1983) 273pp.

22 Kabata-Pendias, A., Agricultural problems related to excessive trace metal contents of soil. In W. Salomons, U. Förstner, & P. Mader (Eds.), Heavy metals (problems and solutions), *Springer-Verlag*, (1995) 3-18.

23 Muller, G., Schwermetalle in den sedimenten des Rheins-Veranderungen seit 1971. *Umschau*, 79 (1979) 778-783.

24 Pearce, J.A. and Norry, M.J., Petrogenetic implications of Ti, Zr, Y, and Nb variations in volcanic rocks, *Contrib. Mineral. Petr.,* 69 (1979) 33-47.

25 Parlak, O., Ho¨ck, V. and Delaloye, M., The supra-subduction zone Pozanti–Karsanti ophiolite, southern Turkey: evidence for high-pressure crystal fractionation of ultramafic cumulates, *Lithos* 65 (2002) 205-224.

26 Nisbet, E.G. and Pearce, J.A., Clinopyroxene composition in mafic lavas from different tectonic settings, *Contrib. Mineral. Petr.,* 63 (1977) 149-160.

27 Kocak, K., Isik, F., Arslan, M. and Zedef, V., Petrological and source region characteristics of ophiolitic hornblende gabbros from the Aksaray and Kayseri regions, central Anatolian crystalline complex, Turkey, *J. Asian Earth Sci.,* 25 (2005) 883-891.

28 Jensen, L.S., A new cation plot for classifying subalkalic volcanic rocks, *Ontario Geological Survey Miscellaneous* ,(1976) Paper 66.

29 Deer, W. A., Howie, R. A. and Zussman, J., An Introduction to the Rock Forming Minerals, 2nd edition, *Longman, London* , (1992) 696pp.

30 Shelley, D., Igneous and Metamorphic rocks under the microscope, *Chapman and Hall*, (1993) 445pp.

31 Morimoto, N., Fabries, J., Ferguson, A.K., Ginzburg, I.V., Ross, M., Seifert, F.A., Zussman, J., Aoki, K. and Gottardi, G., Nomenclature of pyroxenes, *Am. Mineral.,*73 (1988), 1123-1133.

32 Meschede, M., A method of discriminating between different types of mid-ocean ridge basalts and continental tholeiites with the Nb-Zr-Y diagram, *Chem. Geol*., 56(1986) 207-218.

33 Sun, S. S., Mc Donough, W.F., Chemical and isotopic-systematics of oceanic basalts: implications for mantle composition and processes. In: A.D. Saunders and M.J. Norry (Eds.), Magmatism in the ocean basins, *Geol. Soc. London Spec. Publ.,* 42 (1989) 313-345.